The Wide-field Imaging Interferometry Testbed (WIIT): recent progress in the simulation and synthesis of WIIT data

Roser Juanola-Parramon, David T. Leisawitz, Matthew R. Bolcar, Stephen F. Maher, Stephen A. Rinehart[a], Alex Iacchetta[b], and Giorgio Savini[c]

[a]NASA Goddard Space Flight Center, 8800 Greenbelt Rd, Greenbelt MD, USA
[b]Institute of Optics - University of Rochester, 275 Hutchison Rd, Rochester NY, USA
[c]University College London, Gower Street, London, UK

ABSTRACT

The Wide-field Imaging Interferometry Testbed (WIIT) is a double Fourier (DF) interferometer operating at optical wavelengths, and provides data that are highly representative of those from a space-based far-infrared interferometer like SPIRIT. This testbed has been used to measure both a geometrically simple test scene and an astronomically representative test scene. Here we present the simulation of recent WIIT measurements using FIInS (the Far-infrared Interferometer Instrument Simulator), the main goal of which is to simulate both the input and the output of a DFM system. FIInS has been modified to perform calculations at optical wavelengths and to include an extended field of view due to the presence of a detector array.

Keywords: double Fourier, spectroscopy, interferometry, space instrumentation

1. INTRODUCTION

WIIT[1] is a 1:150 functional scale model of the space far-IR interferometer SPIRIT,[2] and is designed to observe complex scenes representative of far-IR astronomical fields. It provides full uv-plane coverage and a wide FOV, operating at visible rather than far-IR wavelengths for several practical reasons: (a) the optical apertures and the delay line are scaled down from those intended for a far-IR instrument in proportion to the wavelength; (b) a CCD detector with sensitivity limited by photon noise (as expected in a cold far-IR space interferometer) was commercially available and affordable; (c) many other parts, such as translation and rotation stages, were available off-the shelf and inexpensive; and (d) a commercial optical metrology system accurate to 10nm was affordable. The novel aspect of WIIT is the use of a detector array (a CCD camera) instead of the single-pixel detector used in a traditional Michelson interferometer. Each pixel on the detector records light arriving from different parts of the sky (test scene). As the delay line is scanned, each pixel records an interferogram unique to the field angle corresponding to the pixel. By using observations at a wide range of uv-positions, obtained by rotating the source and increasing/decreasing the interferometric baseline length, reconstructed images can be produced for each pixel; these images can then be mosaiced together, producing a wide field-of-view image with the full interferometric angular resolution.

The Far-infrared Interferometer Instrument Simulator, FIInS, is an instrument simulator for a Far-infrared Spectro-Spatial Interferometer[3] developed using Matlab. Its main purpose is to simulate both the input and the output of such a system, enabling comparison the input sky map with the synthesised one after some data processing algorithms have been applied. The simulator presents a modular design for the testing of individual

E-mail: roser.juanola@nasa.gov

Optical and Infrared Interferometry and Imaging V, edited by Fabien Malbet, Michelle J. Creech-Eakman, Peter G. Tuthill, Proc. of SPIE Vol. 9907, 990740
 · doi: 10.1117/12.2232090

steps of the spectro-spatial interferometry technique, allowing intermediate outputs to be studied. From a global point of view, the simulator is divided into a sky generator module and an instrument group of modules. The output of FIInS is then processed to reconstruct the sky map. For the simulation of WIIT, FIInS has been modified to perform the calculations at optical wavelengths and with an extended field of view due to the presence of the detector array.

2. SIMULATION OF WIIT DATA WITH FIINS

The first step to simulate a WIIT measurement with FIInS is to define the input sky map or test scene. This input test scene is extracted from the scene definition provided to the experiment light source, the Calibrated Hyperspectral Image Projector[4] (CHIP). CHIP utilizes two Digital Light Processing (DLP) projectors to create custom, spectrally diverse and spatially complex scenes. The two DLP engines (a spectral engine and a spatial engine) operate in series to produce the scene to be measured. First, a broadband source is dispersed onto the digital micromirror device (DMD) of the spectral engine such that individual columns of the mirror are mapped to individual wavelengths. By turning the mirrors in a single column on, the user includes that specific wavelength in the output. The number of on mirrors in a column determines the relative intensity of the spectral component. By selecting numerous columns and appropriately weighting the various spectral components, the user generates a basis spectrum of the hyperspectral scene to be projected. CHIP is capable of producing arbitrary spectra in the band between 380nm and 780nm with a spectral resolution of up to 5nm.

The results presented here correspond to a scene which consists, spatially, of 4 reference point sources, 4 reference binary sources, and 6 extended science sources and is shown in Fig. 1 (left). Fig. 1 shows zoomed in versions of the top reference sources and the science sources. The reference sources are intended to be point sources from the instrument point of view, hence they are 2 by 2 pixels in size, which corresponds to approximately 0.3 arcseconds as it is explained in the next section. The diameter of the science sources is 6 pixels, corresponding to approximately 1 arcsecond.

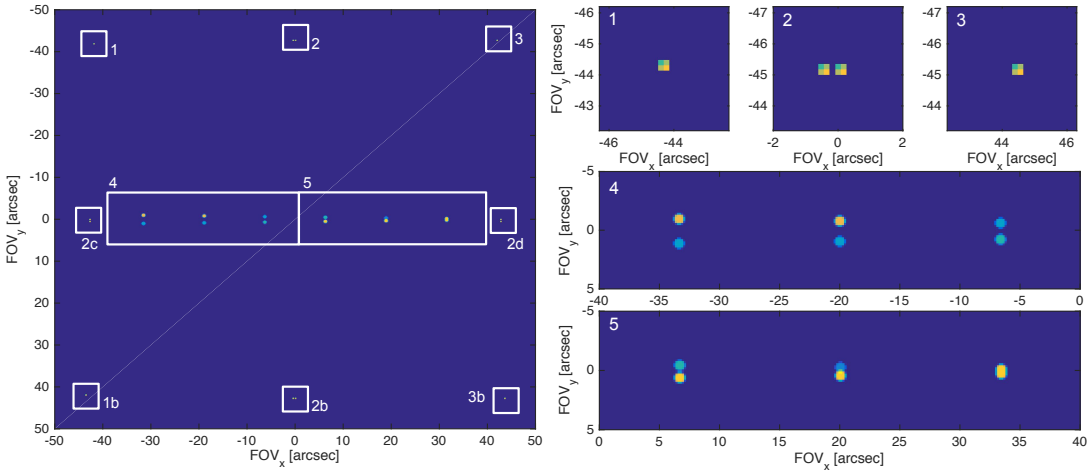

Figure 1. Spatial structure of the input scene at 523.6nm. Left: full scene comprised of 4 referenece point sources (1, 3, 1b, 3b), 4 reference binary sources (2, 2b, 2c, 2d), and 6 science sources (box 4 and 5) which consist of binary extended sources with a 6 pixel diameter with decreasing separation. Right: zoomed view of source 1, 2 and 3 (top row); zoomed view of box 4 (middle row); zoomed view of box 5 (bottom row).

The spectra corresponding to each source, or pair of sources, have been measured in the lab with a spectrograph and are shown in Fig. 2. For the reference sources, our goal is to have as much power being emitted by CHIP as possible, and this can be achieved by configuring CHIP so all the mirrors are 'on' spectrally. For the science sources, 5 different basis spectra are used: a broadband spectrum centred at 600nm (bottom row, which corresponds to the zoomed scene 5, red), the same spectrum including an emission line at 621nm (middle row left and centre, which corresponds to the zoomed scene 4, blue), a lower intensity broadband spectrum centred at 500nm (bottom row, 5 centre, blue), and the same spectrum including an emission line with different intensities (middle row and bottom left panel). This test scene, the spatial and spectral resolution of which is much higher than what the WIIT instrument can measure, is included in the simulator as a FITS file and is consequently interpolated to meet the instrument specifications in order to minimize the computation requirements.

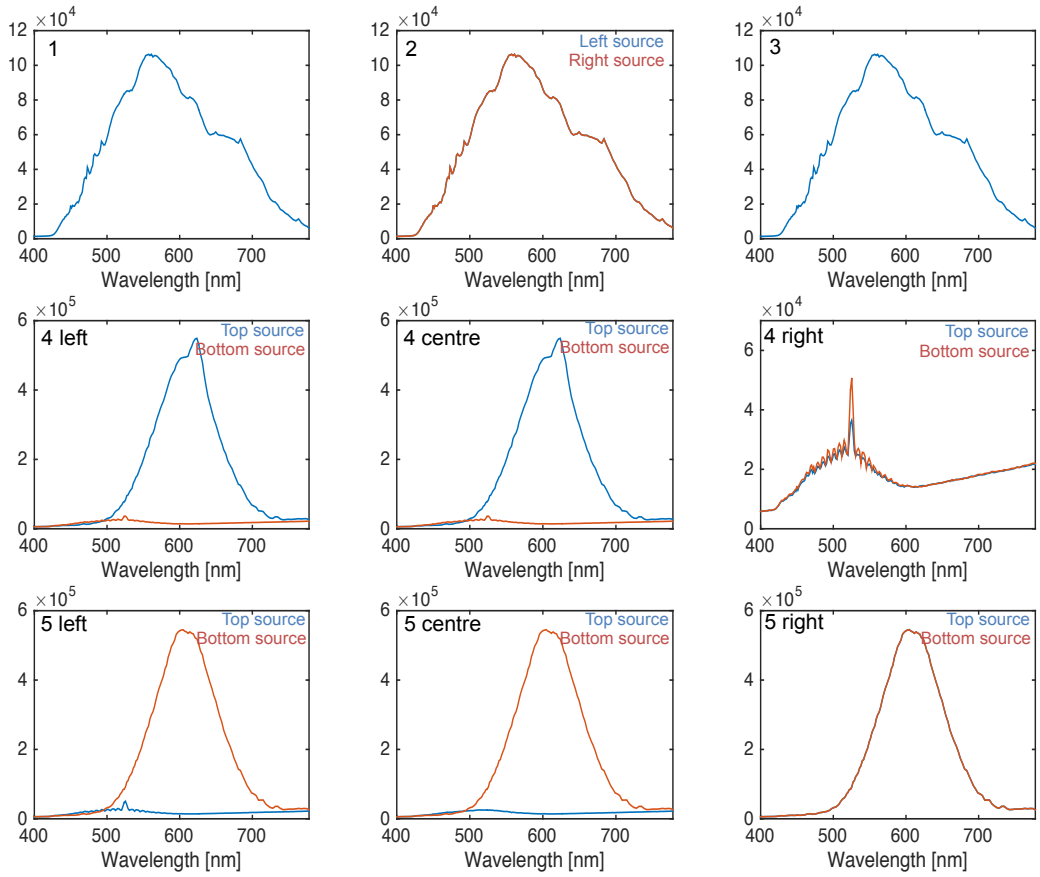

Figure 2. Spectra of each source of the input scene. Top: reference point source 1; reference binary source 2, which present an identical spectrum; reference point source 3. Middle: spectra of the science sources contained in box 4. Bottom: spectra of the science sources contained in box 5. Science sources 5 right present identical spectrum.

2.1 Simulation parameters

The simulator FIInS has been configured as a double Fourier interferometer. Spectrally, a band from 380 nm to 782 nm is assumed, with a minimum spectral resolution of $R = 200$. The simulator calculates 4 OPD samples per fringe, resulting in an OPD step of approximately 50nm.

Spatially, a minimum baseline of 36mm and a maximum baseline of 226mm is set, with a baseline increment of 10mm to match the parameters of a recent experiment conducted with WIIT. The interferometer plane rotates with respect to the input scene such that the the arc length between consecutive rotations for a given baseline length remains constant, providing a grid-style sampling of the uv-map.

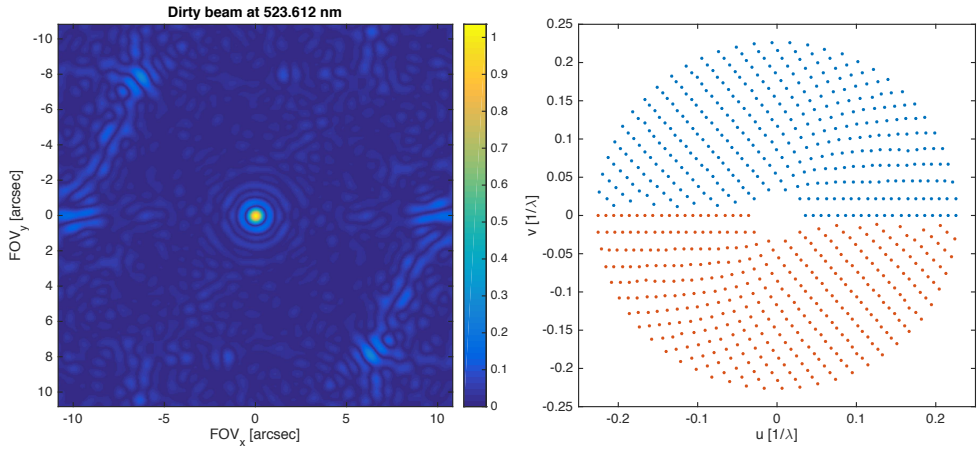

Figure 3. Left: Normalized interferometric dirty beam at 523.6nm. Right: uv-coverage, where blue indicates the sampled uv positions and red its negative counterpart.

Fig.3 (right) shows the sampling of the uv-map. The corresponding interferometric dirty beam at 523.6nm is shown in Fig. 3 (left). It can be observed that the dirty beam pattern is similar to the airy pattern at the centre of the field of view, but presents some distortion with a power level comparable to that of the secondary lobe of the dirty beam. This distortion is due to the fact that the sampling of the uv-map is not completely uniform.

Regarding the optical system, the entrance pupil of WIIT comprises the two apertures of 25mm diameter that constitute the interferometric baseline. The optical system that projects the light on the CCD camera has an F/# of 80, and the CCD pixel size is Δx=16μm, which results in a camera focal length of 2m. With these parameters one can define the focal plate scale (FPS) as FPS = Δx/f = 1.6 arcsec/pixel. Hence, the Airy pattern is oversampled with respect to the Nyquist sampling by a factor of 2.4 to 4.8 at 380nm to 780 nm, respectively.

2.2 Simulation results: WIIT camera plane

The simulator FIInS generates a set of FITS files, more specifically 364 files (one per baseline angle and rotation), each 38.2MB, that contain the simulated datacube. A simulated datacube corresponding to the output of WIIT is a set of 68 x 85 pixel frames, one frame per sampled optical path length for a given baseline. With this current configuration, this means 826 frames per cube.

Fig. 4 (left) shows the integrated intensity for the current simulation with a 226mm baseline length. It can be observed that the binary sources are not resolved spatially, as expected, because the footprint of a single camera pixel is bigger than the angular separation of the binary sources. Fig. 4 (right) shows the cross section of the integrated intensity along the vertical pixels v=9 (top) and v=34 (bottom).

One can display the simulated interferograms by plotting the pixel intensity as a function of the OPD. Fig. 5 shows the interferograms generated for the reference sources (top) and the science sources (bottom) with a baseline of 86mm (left) and 226mm (right) and a rotation of 0 degrees with respect to the CHIP scene. Longer

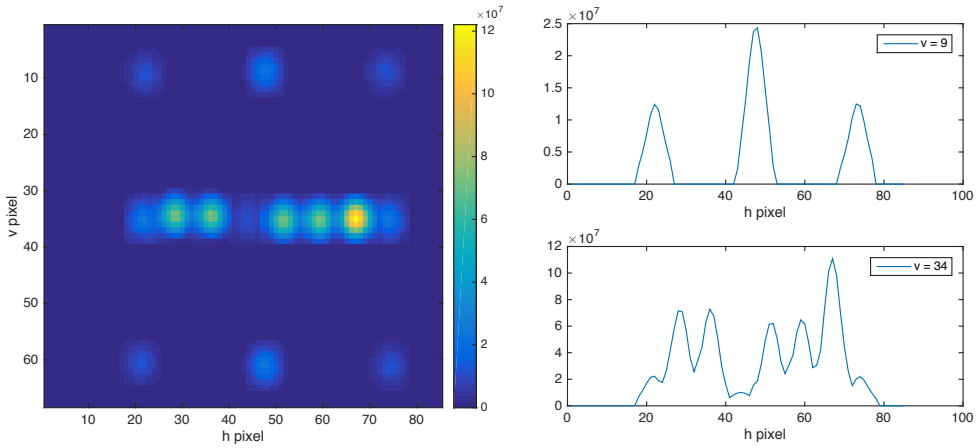

Figure 4. Left: Simulated integrated intensity of a WIIT measurement at the camera plane. Right: cross section of the integrated intensity along the vertical pixel v=9 (top) which corresponds to the references sources, and cross section of the integrated intensity along the vertical pixel v=34 which corresponds to the science sources.

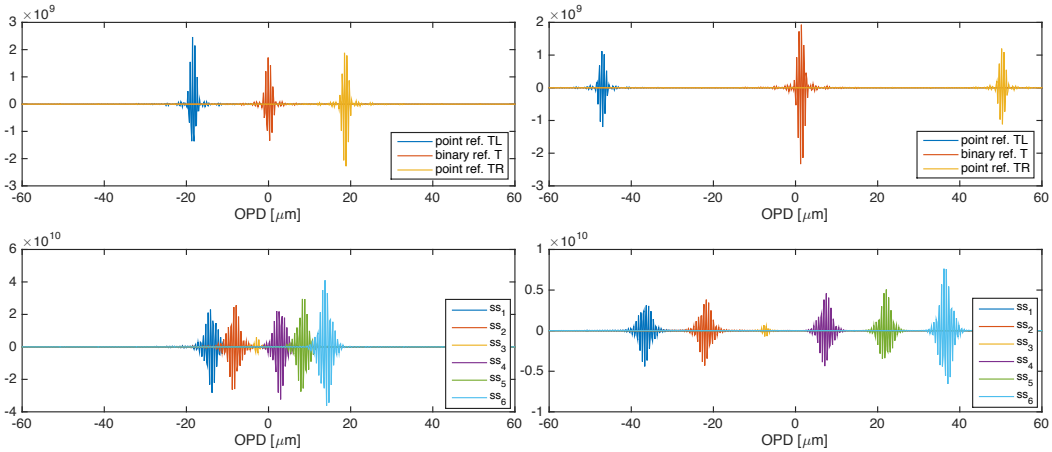

Figure 5. Interferograms generated for the reference sources (top) and the science sources (bottom) with an interferometric baseline of 86mm (left) and 226mm (right) and a rotation of 0 degrees with respect to the CHIP scene.

baselines induce a bigger shift of the centre of the fringe packet (zero path difference location, ZPD) of each interferogram, given by $d_{ZPD} = b \sin\theta$.

From the simulation one can also observe the strong effect the emitted total intensity per source has in the amplitude of the recorded interferogram, i.e. comparing science source 1 with science source 3. In this situation, one can expect that in noisy environments source 3 will not be detected, hence there is a limit in the detectability with a double Fourier modulation instrument which will be further studied quantitatively.

3. RECONSTRUCTION OF THE INPUT SCENE

Once the interferograms have been simulated the next step is to extract the spatial and spectral information for each pixel of the datacube. Because each pixel on the detector plane acts as a single double Fourier interferometer, the single pixel data processing can be applied to the full array as a set of individual pixels.

The reconstruction of the WIIT scene from the recorded interferograms is a two-step process: a spectral inverse Fourier transform, and a spatial inverse Fourier transform. For a given camera pixel (v,h), the 'dirty' spectra $S_{v,h}(\nu, b_j)$ are extracted from the set of interferograms $I_{v,h}(\delta, b_j)$ for each baseline using Eq. 1:

$$S_{v,h}(\nu, b_j) = \sum_{i}^{N} I_{v,h}(\delta_i, b_j) \exp(-i2\pi\nu\delta_i) d\delta \tag{1}$$

The next step is the extraction of the spatial features of $S_{v,h}$; this is the dirty data cube, $Sky_{v,h}$. This step converts a single pixel from each baseline into a datacube covering the angle subtended by the FWHM of the telescope beam (or entrance pupil Airy pattern). To extract the spatial features, one has to perform the two-dimensional Fourier transform of the uv-map. Combining each baseline position b_j and each wavenumber ν_k , the dirty data cube is calculated as

$$Sky_{v,h}(\theta_x\theta_y; \nu_k) = \sum_{j=1}^{Nb} |Im\{S_{v,h}(\nu_k, b_j)\} \cos(2\pi(u_{j,k}\theta_x + v_{j,k}\theta_y)) - Re\{S_{v,h}(\nu_k, b_j)\} \sin(2\pi(u_{j,k}\theta_x + v_{j,k}\theta_y))\} | \tag{2}$$

where $u_{j,k} = b_{x,j}\nu_k$ and $v_{j,k} = b_{y,j}\nu_k$ are the spatial frequencies. In this operation, prior knowledge of the sky grid (θ_x, θ_y) has to be used to mosaic the individual $Sky_{v,h}$ data cubes and reconstruct the wide-field scene.

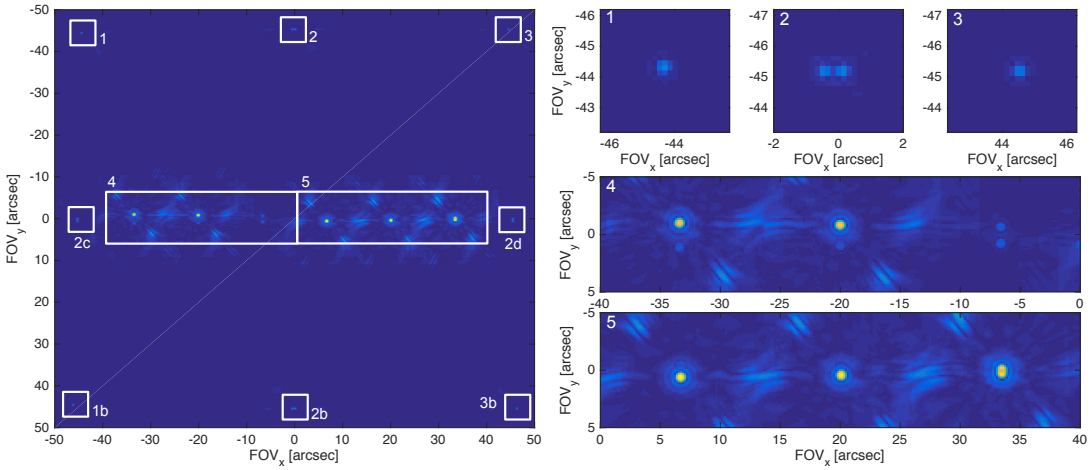

Figure 6. Spatial structure of the reconstructed scene or dirty image. Left: spectrally integrated intensity of the full scene comprised of the 4 referenece point sources (1, 3, 1b, 3b), 4 reference binary sources (2, 2b, 2c, 2d), and 6 science sources (box 4 and 5). Right: zoomed view of source 1, 2 and 3 (top row); zoomed view of box 4 (middle row); zoomed view of box 5 (bottom row).

Fig. 6 shows the spatial distribution of the reconstructed scene or dirty image: the full scene (left) and selected sources (right). Spatially, all the sources are resolved, but one can observe the distortions induced by the dirty beam, with sidelobe power comparable to that of the dimmer sources. By applying post-processing algorithms such as CLEAN[5] and MEM,[6] these artifacts will be minimized.

The derived spectra are in good but not perfect agreement with the known input spectra, as shown in Fig. 7. In the cases where one of the extended sources is substantially more intense than its companion, there is a transfer of power from the brighter to the fainter source at longer wavelengths. This is due to the fact that the width of the interferometric dirty beam is bigger at longer wavelengths (Fig. 7 4 left, 4 centre, 5 left, 5 centre).

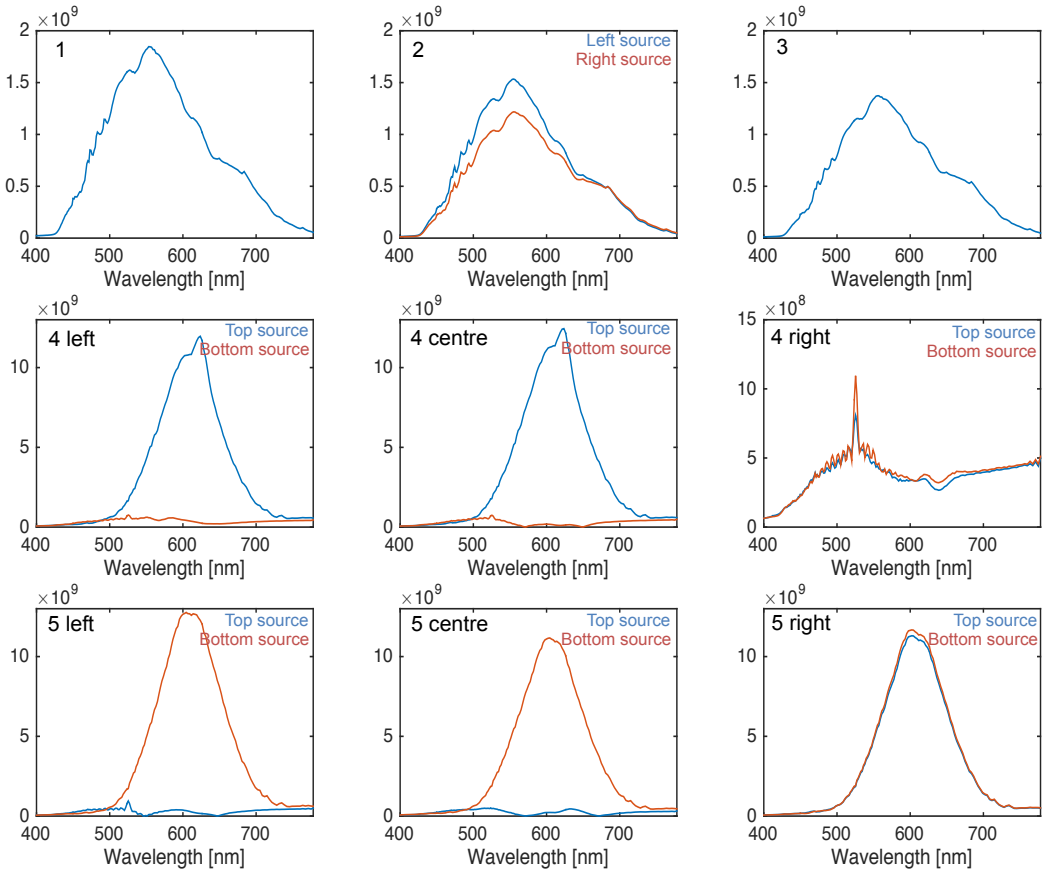

Figure 7. Derived spectra of each source in the scene. Top: reference point source 1; reference binary source 2; reference point source 3. Middle: spectra of the science sources contained in box 4. Bottom: spectra of the science sources contained in box 5.

4. CONCLUSIONS

In this paper we have shown the current status of the simulation of WIIT data and its synthesis. For this purpose, the double Fourier interferometer simulator FIInS has been modified to allow for a detector array to be included in the system, hence extending the field of view. The data synthesis algorithms have been modified to account for this extension of the field of view by mosaicing the synthesized datacube from each pixel on the detector.

FIInS, which can simulate a space-based far-IR interferometer, can further be modified for different optical designs, as new input parameters have been added (i.e. system F-number, pixel pitch, number of detector pixels, etc).

Current efforts are focused on applying data processing algorithms such as CLEAN and MEM to the dirty image to correct for the transfer of power between sources. These algorithms will be tested with simulated data initially and then be applied to the WIIT measured data. Further, new algorithms will be developed to account for the rotation and shift of the scene with respect to the instrument axis in measured data.[7]

ACKNOWLEDGMENTS

This research was supported by an appointment of the lead author to the NASA Postdoctoral Program at the Goddard Space Flight Center, administered by USRA through a contract with NASA.

REFERENCES

[1] Leisawitz, D. T., Bolcar, M. R., Lyon, R. G., Maher, S. F., Memarsadeghi, N., Rinehart, S. A., and Sinukoff, E. J., "Developing wide-field spatio-spectral interferometry for far-infrared space applications," in [*Society of Photo-Optical Instrumentation Engineers (SPIE) Conference Series*], *Society of Photo-Optical Instrumentation Engineers (SPIE) Conference Series* **8445** (2012).

[2] Leisawitz, D., Baker, C., Barger, A., Benford, D., Blain, A., Boyle, R., Broderick, R., Budinoff, J., Carpenter, J., Caverly, R., Chen, P., Cooley, S., Cottingham, C., Crooke, J., Dipietro, D., Dipirro, M., Femiano, M., Ferrer, A., Fischer, J., Gardner, J. P., Hallock, L., Harris, K., Hartman, K., Harwit, M., Hillenbrand, L., Hyde, T., Jones, D., Kellogg, J., Kogut, A., Kuchner, M., Lawson, B., Lecha, J., Lecha, M., Mainzer, A., Mannion, J., Martino, A., Mason, P., Mather, J., McDonald, G., Mills, R., Mundy, L., Ollendorf, S., Pellicciotti, J., Quinn, D., Rhee, K., Rinehart, S., Sauerwine, T., Silverberg, R., Smith, T., Stacey, G., Stahl, H. P., Staguhn, J., Tompkins, S., Tveekrem, J., Wall, S., and Wilson, M., "The space infrared interferometric telescope (SPIRIT): High-resolution imaging and spectroscopy in the far-infrared," *Advances in Space Research* **40**, 689–703 (2007).

[3] Juanola-Parramon, R., Fenech, D., and Savini, G., "Architecture and performance of the space-based far-infrared interferometer instrument simulator," *Monthly Notices of the Royal Astronomical Society* **457**(4), 3457–3469 (2016).

[4] Bolcar, M. R., Leisawitz, D. T., Maher, S. F., and Rinehart, S. A., "Demonstration of the Wide-field Imaging Interferometer Testbed using a Calibrated Hyperspectral Image Projector," in [*Society of Photo-Optical Instrumentation Engineers (SPIE) Conference Series*], *Society of Photo-Optical Instrumentation Engineers (SPIE) Conference Series* **8445** (2012).

[5] Högbom, J., "Aperture synthesis with a non-regular distribution of interferometer baselines," *Astron. Astrophys. Suppl* **15**(1974), 417–426 (1974).

[6] Gull, S. and Skilling, J., "Maximum entropy method in image processing," *Communications, Radar and Signal Processing, IEE Proceedings F* **131**(6), 646–659 (1984).

[7] Alexander S. Iacchetta, J. R. F. and Leisawitz, D. T., "Rotation and translation registration of bandlimited interferometric images using a chirp z-transform," in [*Proc. SPIE*], *Society of Photo-Optical Instrumentation Engineers (SPIE) Conference Series* **9907** (2016).